Acidic Residues on the Voltage-Sensor Domain Determine the Activation of the NaChBac Sodium Channel

Jonathan Blanchet, Sylvie Pilote, and Mohamed Chahine
Research Centre and Department of Medicine, Hôpital Laval, Quebec City, Quebec, Canada G1V 4G5

ABSTRACT The voltage-sensing domain of voltage-gated ion channels is characterized by specific, conserved, charged residues. Positively charged residues on segment S4 are the main contributors to voltage-sensing and negatively charged residues on the S2 and S3 segments are believed to participate to the process. However, their function in the voltage sensor is not well understood. To probe the role of three acidic residues in NaChBac (D-58 and E-68 in S2, and D-91 in S3), we employed site-directed mutagenesis to substitute native acidic residues with cysteine (neutral), lysine (positive charge), or either aspartate or glutamate (negative charge). We used a combination of the patch-clamp technique to record Na^+ currents and molecular modeling to visualize interacting amino acid residues. We suggest that the acidic residues on the S2 and S3 segments form specific interactions with adjacent amino acids in the voltage-sensor domain. The main interactions in NaChBac are D-58 (S2) with A-97-G-98 (S3) and R-120 (S4), E-68 (S2) with R-129 (L4-5), and D-91 (S3) with R-72 (S2). Changing these acidic residues modified the interactions, which in turn altered the sensitivity of the voltage sensor.

INTRODUCTION

Voltage-gated ionic channels are membrane proteins involved in the transport of ions in both prokaryotic and eukaryotic cells (1). They belong to a large family of proteins that includes several types of voltage-gated Na^+, Ca^{2+}, and K^+ channels. NaChBac is a prokaryotic voltage-gated Na^+ channel from *Bacillus halodurans* (2). NaChBac was recently cloned and has some remarkable features. For example, even though the channel is Na selective, the amino acid sequence of the selectivity filter is similar to that of calcium channels. It is a homotetramer and each monomer is composed of six transmembrane segments (S1–S6) (3). The S1–S4 domain makes up the voltage-sensor domain, whereas the linker between S5 and S6 forms the pore of the channel (4). According to the crystal structures of K^+ channels, the voltage-sensor domain is almost independent of the pore (5). This is in agreement with recent discoveries of voltage-sensor proteins that are not attached to a pore domain or that are attached to phosphoinositide phosphatase (6–8).

Regardless of the origin of the voltage sensor, it has been shown that several charged residues are conserved in segments S2, S3, and S4. S4 segments usually have four or more basic residues–most of them arginine residues (9)–which are involved in the voltage-sensing process. The role of these arginine residues has already been studied in NaChBac (10). Three conserved acidic residues in the S2 and S3 segments are also believed to participate in the gating process of the *Shaker* K^+ channel by interacting via positively charged residues in S4 (11–13). These three residues are also present in NaChBac. The charge conservation of these residues in voltage sensors in different species is consistent with the view of a divergent structural evolution (14).

It has been suggested that electrostatic network interactions exist between acidic groups on S2 and S3 and basic residues on S4 in the *Shaker* K^+ channel, but this hypothesis has been challenged recently (15,16). Experimental results suggest that two networks of strong, local, electrostatic interactions stabilize the structure of the channel and play an important role in activation. One is E-283(S2):R-368(S4):R-371(S4) and the other, E-293(S2):D-316(S3):K-374(S4) (13). The isolated voltage-sensor crystal structure does not clearly show these interactions (17). Indeed, homologous residues of the *Shaker* E-283 (D-62 in KvAP) do not interact strongly with R3 or R4, the third and the fourth arginine residue in the S4. Moreover, no residues in S4 interact with D-72 or E-93 in KvAP, the homologous residues to E-293 and D-316 in the *Shaker* K^+ channel. However, the crystal structure does not rule out the possibility of these interactions because they may occur in the closed conformation of the voltage sensor, which has not yet been structurally determined. Nevertheless, other studies suggest that a direct electrostatic interaction between these charged residues is not consistent with the gating process (15,16) because such an interaction would neutralize the arginine residues in S4 and eliminate the voltage-sensing capacity. They also suggest that breaking these interactions during gating could create a high-energy barrier, but there is some uncertainty about the real energetic cost of breaking salt bridge interactions since they appear to naturally break and reform in proteins (18,19).

In this work, we studied the interactions involved in the voltage-gating process of NaChBac by exploring the role of acidic residues in the S2 and S3 segments. To do this, we

Submitted June 3, 2006, and accepted for publication December 27, 2006.

Address reprint requests to Mohamed Chahine, PhD, Le Centre de recherche Université Laval Robert-Giffard, Local F-6539, 2601 chemin de la Canardière, Québec (Québec) G1J 2G3 Canada. Tel: 418-663-5747 ext. 4723; Fax: 418-663-8756; E-mail: mohamed.chahine@phc.ulaval.ca.

0006-3495/07/05/3513/11 $2.00

doi: 10.1529/biophysj.106.090464

used site-directed mutagenesis to change these residues (D-58 and E-68 in S2, and D-91 in S3) into cysteine (neutral charge), lysine (positive charge), and aspartate or glutamate (negative charge) to study their effect on activation. We also built a homology model base on the recently determined crystal structure to better understand the nature of the inter-residue interactions and how they influence the gating process.

MATERIALS AND METHODS

Site-directed mutagenesis and recombinant DNA construction

Recombinant cysteine mutants of the three acidic residues were generated using QuickChange site-directed mutagenesis kits from Stratagene (La Jolla, CA) according to the manufacturer's instructions and as previously described (10). The presence of the mutations was confirmed by automatic sequencing of the entire NaChBac gene (CHUL Research Centre DNA sequencing facility, Quebec City, QC, Canada). WT and mutant NaChBac and CD8 were constructed in the piRES vector (piRES/CD8/NaChBac). For the patch-clamp experiments, 2- to 3-day posttransfection cells were incubated for 5 min in a medium containing anti-CD8-a-coated beads (Dynabeads M-450 CD8-a, Dynal Biotech ASA, Oslo, Norway) as previously described (20). Cells expressing surface CD8-a fixed the beads and were visually distinguishable by light microscopy from nontransfected cells (21).

Transfections of the tsA201 cell line

TsA201, a mammalian cell line derived from human embryonic kidney (HEK) 293 cells, was grown and incubated as previously described (10,20).

Patch-clamp method

NaChBac macroscopic Na^+ currents from tsA201-transfected cells were recorded using the whole-cell configuration of the patch-clamp technique as previously described (10).

Solutions and reagents

For whole cell recordings, the patch pipette contained 35 mM NaCl, 105 mM CsF, 10 mM EGTA, and 10 mM HEPES-free acid. The pH was adjusted to 7.4 using 1 N CsOH. The bath solution contained 150 mM NaCl, 2 mM KCl, 1.5 mM $CaCl_2$, 1 mM $MgCl_2$, 10 mM glucose, and 10 mM HEPES-free acid. The pH was adjusted to 7.4 with 1 N NaOH. The liquid junction potential between the patch pipette and the bath solutions was corrected by −7 mV. The recordings were made 5 min after obtaining the whole cell configuration to allow the current to stabilize and the contents of the patch electrode to diffuse adequately. Experiments were carried out at room temperature (22°C–23°C).

Statistical analyses

Data are expressed as mean ± SE (standard error of the mean). When indicated, a *t*-test was performed for biophysical parameters using statistical software SigmaStat for Windows v3.00 (Systat Software, Point Richmond, CA). Time constant data were analyzed by a posteriori Dunett comparisons with SAS software (SAS Institute, Cary, NC). Differences were deemed significant at $p < 0.05$.

Data analyses

The Na^+ channel conductance (G) was calculated from peak currents (I) according to the following equation $G = I/(V - V_{Na})$, where V is the test potential and V_{Na} is the reversal potential determined by the intercept of the linear interpolation of the current before and after reversal. The data points of the G-V curve were fitted using the Boltzmann equation $G/G_{max} = 1/(1 + \exp[(V - V_{½})/k_v])$, where G is the measured conductance, k_v represents the slope factor, $V_{½}$ is the potential at which the half maximal channel open probability occurs, and G_{max} is the maximal conductance.

Homology modeling

The crystal structure of the KvAP-isolated voltage sensor (1ORS in the Protein Data Bank) was used to build the NaChBac model by homology modeling (17). It was chosen over Kv1.2 structure mainly because of its better resolution (see Supplementary Material (I) for more details). Two sequence alignments were performed before modeling, one with ClustalW (22) and another with T-Coffee (23). A comparison of alignments gave different results for S3 and S4, where the four arginine residues in NaChBac were shifted with T-Coffee relative to their homologous positions in KvAP and Kv1.2 (Fig. 1). Both models were built to explore the impact of shifting the arginine residues on interactions. Only the activated conformation of the voltage sensor was considered during the modeling since it is the conformation adopted by the isolated voltage-sensor structure of KvAP (17). De novo building of the resting conformation was not attempted for this study because we lack too many structure-function data that should restrict the numerous conformation possibilities, in addition to the uncertainty surrounding the voltage sensor's displacement during gating. Moreover, since the biophysical effects studied here concern mainly the channel activation, a structure of the activated conformation is more relevant.

Homology modeling, calculations, and structure optimizations were performed with the ZMM program (www.zmmsoft.com) (24,25). Atom-atom interactions were calculated using the AMBER force field (26) with a cutoff distance of 8 Å and a shifting function (27). Electrostatic interactions were calculated using the distance-dependent dielectric. Solvation effects were taken into account using an implicit-waters method (28). Counterions were not added to the models because their positions in the original structure are not known. With these conditions the software might overestimate the relative force of electrostatic interactions; for example, salt bridges will show large energy values compared to other interactions. Therefore, these values need to be interpreted with caution. Conformational searches and optimization of the models were done with the Monte Carlo minimization protocol (29–31). In every calculation, C_α atoms of conserved residues were restrained to 1 Å from their crystallographic coordinates with a flat-bottom energy function. A complete description of the model building is provided in the Supplementary Material (I).

RESULTS

Biophysical characterization of the S2 and S3 acidic residue mutations

Role of the S2 and S3 acidic residue on activation

The biophysical characterization included analyses of the families of Na^+ current-voltage relationships, the G-V curves, and the time constants of activation and inactivation. Examples of a family of Na^+ currents for wild-type (WT) and D-58 mutant NaChBac channels are shown in Fig. 2, *A–D*. Neutralizing the aspartate residue at position 58 (D-58C) on the S2 transmembrane segment resulted in a shift of the G-V curve to a more positive potential (Fig. 2 *E*).

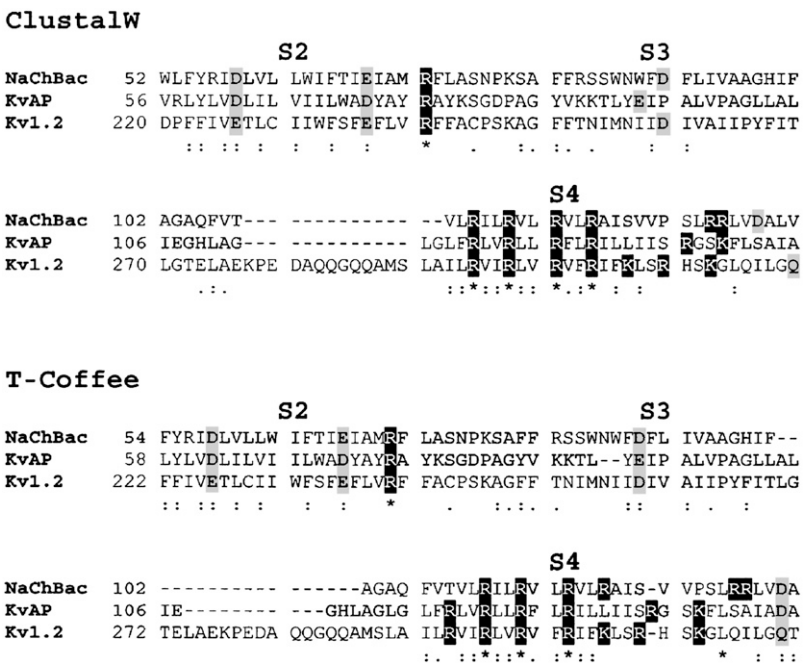

FIGURE 1 Sequences alignment of segments S2, S3, and S4 of NaChBac, KvAP, and Kv1.2 performed with ClustalW (22) and T-Coffee (23). Both alignments suggest a shorter paddle or S3 segment in NaChBac as previously reported (40). Legend: ''.'' semiconserved residue; '':'' conserved residue; ''*'' same residue. Highlighting of conserved or important residues: black (basic/positive residue), shaded (acidic/negative residue).

A similar result was obtained when a positive charge (K) replaced the negative charge of the native aspartate residue. Conserving the negative charge (D to E) resulted in a modest but statistically significant left shift of the G-V curve to more negative potentials (Fig. 2 *E*) (see Table 1 for G-V parameters and the bar diagram on Fig. 3).

Examples of a family of Na^+ currents for E-68 mutant NaChBac channels are shown in Fig. 4, *A–C*. Unlike the D-58 mutations, neutralizing or replacing the negative charge by a positive charge at position 68 (E-68C or E-68K) on the S2 transmembrane segment resulted in a shift of the G-V curve to more negative potentials (Fig. 4 *D*).

Examples of a family of Na^+ currents for D-91 mutant NaChBac channels are shown in Fig. 5, *A–C*. Like the E-68 mutations, neutralizing as well as reversing the negative charge at position 91 on the S3 segment (D-91C or D-91K) shifted the G-V curve to more negative potentials, whereas conserving the negative charge shifted the G-V curve to more positive potentials (Fig. 5 *D*) (see Table 1 for G-V parameters and the bar diagram in Fig. 3).

Thus, positive or neutral mutants of D-58 led to channels that were less sensitive to changes in voltage, whereas a change in E led to a more sensitive channel. This is demonstrated by a shift in the $V_{1/2}$ and significant changes in the slop factor (Table 1). On the other hand, E-68 and D-91 mutants were more sensitive when the negative charge was changed to a positive or neutral charge, whereas it was less sensitive when changed to another type of negative charge. Although E-68 and D-91 are located on two different transmembrane segments, the similar biophysical phenotypes observed with these two residues suggest that they may interact with the same residues or may have the same influence on the same interacting region.

Role of the S2 and S3 acidic residues in modulating the kinetics of activation and inactivation

For D-58 mutants, there were no significant changes in the kinetics of activation, but the time constants of inactivation were significantly slower than that of the WT (data not shown). Interestingly, the presence of a neutral (C) or a positive (K) charge at position 68 resulted in slower activation kinetics and slow entry into the inactivated state (Fig. 6, *A* and *B*). This was reflected by slower current decay time constants. For D-91 mutants, slight changes in the kinetics of activation and inactivation were observed (Fig. 6, *C* and *D*). This suggests that D-58 and E-68 may influence the way the channel pore collapses.

Homology models of the voltage-sensor domain

WT NaChBac models built using T-Coffee and ClustalW gave similar results. These models gave a similar systemic energy, the main interactions were almost the same, the energy contributions of the residues were on the same order of magnitude and the same changes were observed when the residues were mutated. The differences between the models involved D-58, which is close to the S4 segment, and E-68, which mainly interacts with R-129 in the T-Coffee model (see below) and R-130 in the ClustalW model (see Supplementary Material (II)). Because showing the analysis of both models in this work might be tedious, we preferred to show only the models obtained with the T-Coffee alignment, where the arginine residues in S4 were shifted (Figs. 1 and 7, *A* and *B*). Our main reasons are that the results obtained from the T-Coffee alignment were easier to compare with the *Shaker* K^+ channel (23) because R-120 (R-4) in NaChBac is

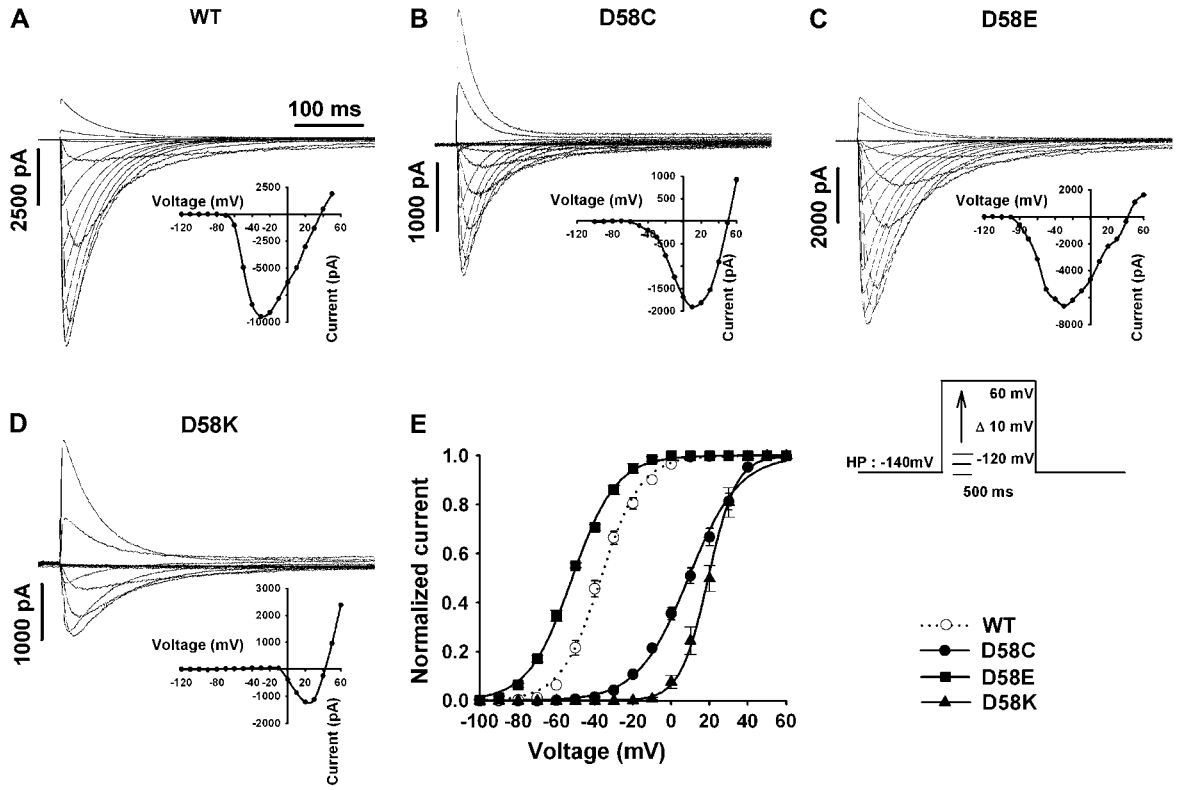

FIGURE 2 Families of whole-cell sodium current traces recorded from tsA201 cells expressing (*A*) NaChBac/WT, (*B*) NaChBac/D-58C, (*C*) NaChBac/D-58E, and (*D*) NaChBac/D-58K. Currents were generated from a holding potential of −140 mV using 500-ms depolarizing steps from −120 to 50 mV in 10-mV increments, as indicated in the center of the figure. The current-voltage relationship (I/V), where the maximum Na^+ current was plotted versus the applied voltage for each current trace, is shown in the inset below the corresponding family of current traces. Voltage dependence of the steady-state activation (G/V) of the NaChBac/WT channel ($n = 13$) and the three D-58 mutants (D-58C ($n = 7$), D-58E ($n = 3$), and D-58K ($n = 7$)) (*E*). The value of the data points are expressed as mean ± SE. See Table 1 for $V_{½}$ and K_v parameters.

homologous to K-5 (K-374) in the *Shaker* K+ channel. Also, the T-Coffee model might better agree with our previous work (10) where R-129C shows a strong effect on gating and inactivation kinetics, which might be explained by its interaction with E-68. Finally, it was presumed that T-Coffee is more accurate than ClustalW for sequences that have <30% identity, which is the case of NaChBac compared to KvAP and Kv1.2. An example of T-Coffee accuracy for our work, ClustalW did not correctly align the conserved acidic residue in S3 (Fig. 1). However, the particularities of the models obtained from ClustalW are interesting and should not be put aside, especially without other proofs of NaChBac's shifted arginine residues in S4. The results and analysis of the ClustalW model are presented in the Supplementary Material (II).

Residue D-58 interacts mainly with the side chain of R-120 and with the backbone of A-97 and G-98 in S3. The respective interaction energies are −7.1, −2.2, and −3.6 kcal·mol^{-1} (Table 2). However, D-58 is too far from S4 to create a salt bridge with R-120 (Fig. 7 *C*). In this model, it appears that R-120 had the same role as K-374 (K-5) in the *Shaker* K+ channel and R-133 in KvAP (Fig. 7 *D*), despite the fact that they are not aligned in Fig. 1. R-133 in KvAP is located one helix turn past (four residues), and thus on the same helix face, R-120 and K-374. The head of the residue's side chain is approximately in the same spatial position and almost forms the same interactions (Fig. 7, *C* and *D*). The difference in the position of R-120 versus R-133 (absence and presence of a salt bridge) could indirectly be a reason for the kinetic and sensitivity differences between both channels. D-58C loses all these interactions, which change the interaction network of the residues in the voltage-sensing domain. This change is reflected by an increase of the interaction energy of the residue, from −20.1 to −4.7 kcal·mol^{-1} (Table 3; Table 4 in Supplementary Material (II)). D-58K also loses the interactions observed in the WT channel, with total interaction energy of −9.4 kcal·mol^{-1}, but it is stabilized by E-41 (Table 3). D-58E, which conserves the negative charge, was closer to S4 and formed a strong salt bridge with R-120, where the interaction energy changed from −7.1 to −32.3 kcal·mol^{-1}, for a difference of −25.2 kcal·mol^{-1}(Tables 2 and 3 and Fig. 7 *E*). Such large changes in interaction energy are most probably exaggerated by the modeling software (see Materials and Methods), but they are representative of a

TABLE 1 Comparative activation biophysical parameters for NaChBac/WT and the mutants D-58, E-68, and D-91

Mutated residues	Activation parameters	Negative charge substitution		
		C	K	E/D†
D-58	$V_{½}$	9.1 ± 1.7* $n = 7$	19.2 ± 1.9* $n = 7$	−51.8 ± 0.1* $n = 3$
	k_v	−13.0 ± 0.5* $n = 7$	−6.8 ± 0.5 * $n = 7$	−11.5 ± 0.5 $n = 3$
D-91	$V_{½}$	−74.6 ± 3.3* $n = 17$	−72.9 ± 2.6* $n = 4$	−18.2 ± 6.4* $n = 5$
	k_v	−15.0 ± 1.0* $n = 17$	−10.2 ± 1.2 $n = 4$	−13.8 ± 0.8* $n = 5$
E-68	$V_{½}$	−83.8 ± 4.1* $n = 5$	−62.5 ± 2.7* $n = 13$	−17.9 ± 2.6* $n = 9$
	k_v	−13.5 ± 1.6* $n = 5$	−16.8 ± 1.0* $n = 13$	−20.8 ± 0.5* $n = 9$

The parameters shown ($V_{½}$ and K_v) were derived from Boltzmann fits to the corresponding steady-state activation curves. The values are expressed as mean ± SE.
n, number of experiments.
$V_{½}$, voltage for half activation.
k_v, slope factor.
*Significantly different ($p < 0.05$) from respective control WT parameters ($V_{½} = -35.9 \pm 1.1$, $k_v = -10.1 \pm 0.4$, $n = 13$).
†E substitution for D-58 and D-91 and D substitution for D-68.

much stronger interaction in the case of salt bridges. D-58E maintained good interactions with A-97 and G-98, but R-120 bound less strongly to L-93, I-94, and A-96 in S3, which were the main interacting residues in the WT model (Fig. 7 *C*). Other mutations of D-58 did not greatly affect the interactions of R-120 with S3 residues.

The main interaction of E-68 in the WT model was a salt bridge with R-129, which strongly bound the C-ter end of S2 helix to the S4-S5 linker (L4-5) with an interaction energy of -36.7 kcal·mol^{-1} (Fig. 7 *F*). It also formed a favorable intrahelix contact (-14.7 kcal·mol^{-1}) with R-72, an interaction that may help stabilize the formation of the helix (Table 2). The proximity of D-91 in S3 and D-133 in L4-5 created a repulsive force (4.7 and 5.1 kcal·mol^{-1}) between E-68 and these residues, respectively. However, unlike E-68, D-91 mainly interacted with R-72 (-24.1 kcal·mol^{-1}) but also had a favorable interaction with R-129 (-5.9 kcal·mol^{-1}) (Fig. 7 *F* and Table 3). This interaction pattern is different from that in KvAP (Fig. 7 *G*), mainly because R-129 (in NaChBac) is located one helix turn farther. In KvAP, K-136 does not form a salt bridge with D-76 or E-93 because it is too far from these residues. However, it is close enough to form stabilizing electrostatic interactions with these residues. E-68C loses all interactions with its environment, which had a significant effect considering the loss of the E-68-R-129 interaction. Changing the residue to a lysine had the same effect, resulting in a loss of all interactions with the environment. Total interaction energy of E-68C and E-68K are relatively close, being -3.3 and 3.7 kcal·mol^{-1}, respectively, compared to -43.9 for the WT (Table 4 in Supplementary Material (II)). It did not, for example, seem to be significantly stabilized by interacting with D-91 (Fig. 7 *H*). E-68D only weakened the interaction of the residue with R-129 (Table 3). D-91 interactions were not significantly affected by these mutations. Only E-68K enhanced the interactions of D-91 with R-72 and R-129. Mutations of D-91 and E-68 exhibited similar characteristics. Mutating D-91 to C or K caused the loss of strong bonds between this residue and R-72, but the salt bridge between E-68 and R-129 was usually present and the E-68-R-72 interaction was stronger (Table 3). D-91E interacted more strongly with R-129 and to a lesser extent with R-72. This mutation slightly weakened the interaction of E-68 with R-72 and R-129 (Fig. 7 *F*).

Interestingly, charge-reversal (negative to positive) mutations resulted in a slight but statistically significant difference in the $V_{1/2}$ values (Table 1) compared to charge neutralization; this was true for D-58 ($p = 0.002$) and E-68 ($p < 0.001$) but not for D-91 ($p = 0.812$). Such a radical change was expected to greatly affect voltage-sensor activity. Molecular modeling showed that the interaction energy of neutralized or charge-reversed residues has almost the same effect on the residue-residue interactions (Table 3). This was the result of a rearrangement of interactions between the voltage sensor and the lysine residue whose positive charge was partially stabilized and almost neutralized.

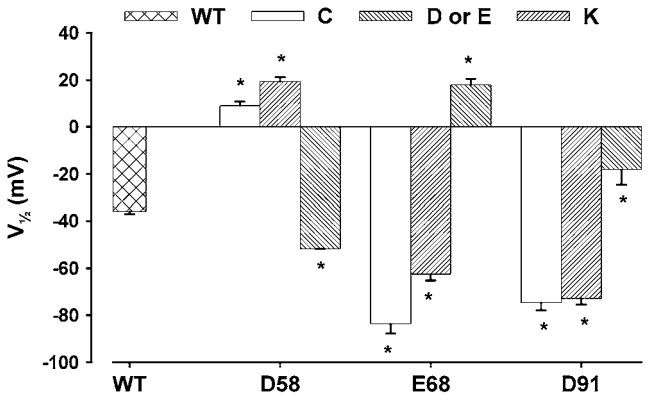

FIGURE 3 Bar diagrams illustrating the effect C, K, D, or E mutations at positions D-58, E-68, and D-91 of NaChBac on the $V_{½}$ values. The $V_{½}$ values were derived from Boltzmann fits of the steady-state activation curves. The values of each bar diagram are expressed as mean ± SE, and significant differences ($p < 0.05$) from the WT are indicated by ''*''.

DISCUSSION

Role of S2 and S3 acidic residues on activation and predicted behavior in a NaChBac model

Our goal was to study the role of the conserved acidic residues in the S2 and S3 transmembrane segments of NaChBac in channel gating. We used site-directed mutagenesis to change these residues into C (neutral), K (positive), or another negatively charged residue (either E or D) and to study the effect

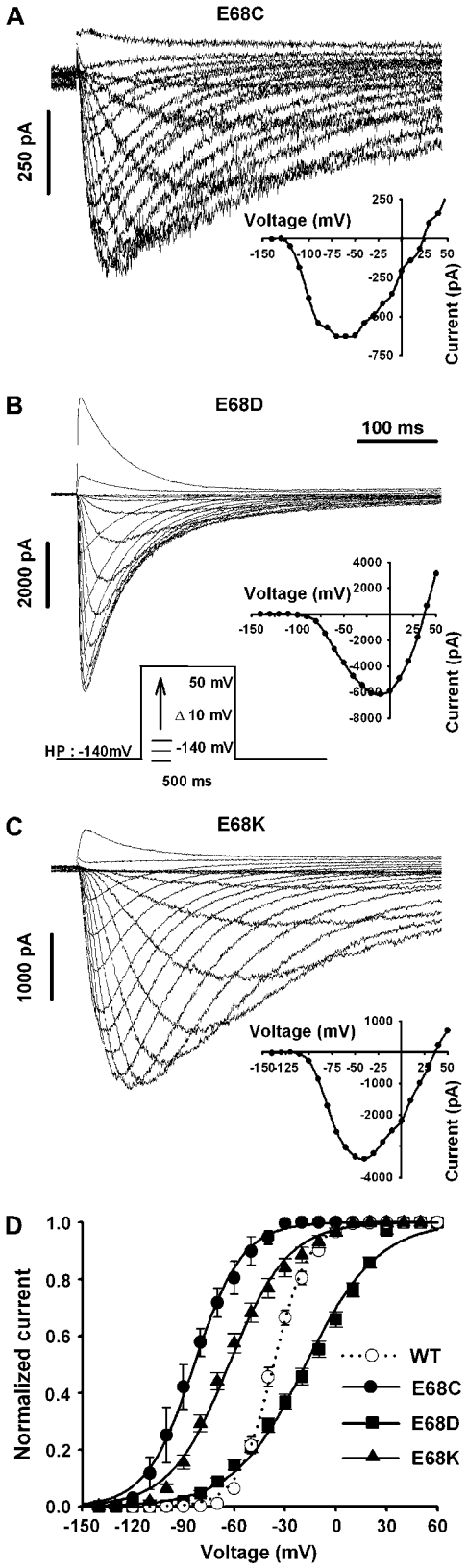

FIGURE 4 Families of whole-cell sodium current traces recorded from tsA201 cells expressing (*A*) NaChBac/E-68C, (*B*) NaChBac/E-68D, and (*C*) NaChBac/E-68K. Currents were generated from a holding potential of −140 mV using 500-ms depolarizing steps from −140 to 50 mV in 10-mV increments as indicated in the center of the figure. The current-voltage relationship (I/V), where the maximum Na^+ current was plotted versus the applied voltage for each current trace, is shown in the inset below the corresponding family of current traces. Voltage dependence of the steady-state activation (G/V) of the NaChBac/WT ($n = 13$) channel and the three E-68 mutants (E-68C ($n = 5$), E-68D ($n = 9$), and E-68K ($n = 13$)) (*D*). The value of the data points are expressed as mean ± SE. See Table 1 for the $V_{½}$ and K_v parameters.

this has on channel activity. Reversing or neutralizing the charge of D-58 shifted the activation midpoint toward a more depolarized potential, suggesting a more stable closed state. In contrast, reversing or neutralizing the charges of E-68 and D-91 shifted the activation midpoint toward more hyperpolarized potentials, suggesting an unstable closed state. This also led to slower current decay. Conserving the charge resulted in a slight shift in the opposite direction compared to other mutations. We also built a molecular model based on the recently crystallized KvAP voltage-gated potassium channel to visualize interresidue interactions and to study the effect on the voltage sensor of changing the charges of the conserved acidic residues. In the models, reversing or neutralizing the charge of one of the three residues led to a loss of the usually strong interactions observed in the WT model. Conserving the charge such as changing D to E led to stronger interactions, whereas changing E to D led to weaker interactions. E differs from D by the presence of an additional CH_2 group in the side chain. This small difference has a significant effect on NaChBac function. Differences between the G/V curves and interaction energies with the mutated residues showed that D-58 behaved differently than E-68 and D-91, which are close to each other and may influence each other's interactions.

Comparison with previous *Shaker* studies

In our study, all the NaChBac mutant channels were functional and thus provided a complete data set. Observations similar to ours are difficult to make with the *Shaker* K+ channel because most *Shaker* mutants do not express functional channels (32). However, most of the available data for *Shaker* mutants are similar to ours. For example, the G/V curves of *Shaker* mutants E-293Q and E-293K were shifted to the left, as was the case with NaChBac mutants E-68C and E-68K. Also, the G/V curve of E-283D was shifted to the right, whereas the G/V curve of D-58E exhibited a slight shift to the left. In both cases, the D residue at this position (the first acidic residue in S2) produced a more depolarized G/V curve than the E residue. There are, however, several differences between the *Shaker* and NaChBac channels that raise questions as to whether the voltage-sensor domains of the two channels have the same interactions and mechanical functions. Despite the well-known conserved residues in S2, S3, and S4, the S4 segment has a different pattern of arginine

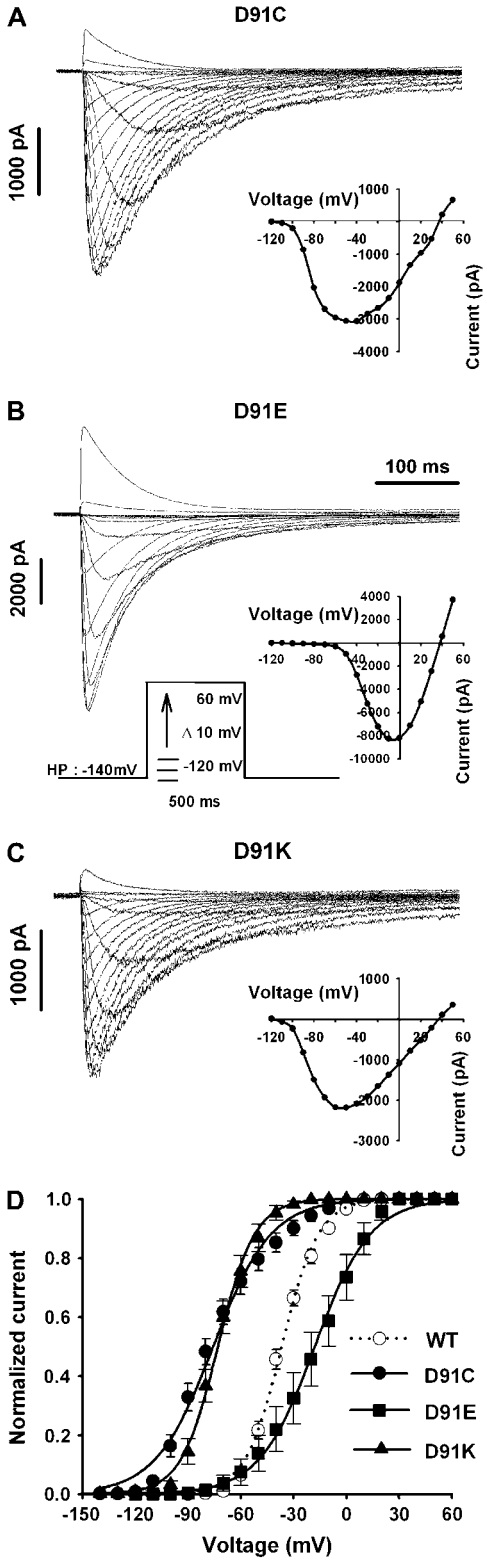

FIGURE 5 Families of whole-cell sodium current traces recorded from tsA201 cells expressing (*A*) NaChBac/D-91C, (*B*) NaChBac/D-91E, and (*C*) NaChBac/D-91K. Currents were generated from a holding potential of −140 mV using 500-ms depolarizing steps from −120 to 50 mV in 10-mV increments as indicated in the center of the figure. The current-voltage relationship (I/V), where the maximum Na^+ current was plotted versus the applied voltage for each current trace, can be seen in the inset below the corresponding family of current traces. Voltage-dependence of the steady-state activation (G/V) of the NaChBac/WT channel ($n = 13$) and the three D-91 mutants (D-91C ($n = 9$), D-91E ($n = 4$), and D-91K ($n = 15$)) (*D*). The value of the data points are expressed as mean ± SE. See Table 1 for $V_{½}$ and K_v parameters.

residues in different channels. In our model, which we obtained with ClustalW (Fig. 1; see also Supplementary Material (II)), the first four arginine residues in NaChBac are aligned with the first four arginine residues of KvAP and Kv1.2. However, NaChBac has no residue that is equivalent to K-374 (*Shaker*) or R-133 (KvAP). With T-Coffee, R-1 is not present in NaChBac and the equivalent of K-374 (*Shaker*) and R-133 (KvAP) is R-120. Can these differences somehow be compensated for or do they have a specific role in their respective channels? Despite the similarities between the studies on *Shaker* and NaChBac channels, it is noteworthy that E-293D in the *Shaker* channel has no effect on the G/V curve whereas mutant E-68D, the equivalent residue in NaChBac, leads to a depolarized shift of the G/V curve. These conserved residues may thus have slightly different functions in different channels.

To the best of our knowledge, only one other structure-based model has looked at acidic residue interactions in S2-S3. In this molecular dynamics simulation of the KvAP voltage sensor, the authors suggested that negatively charged residues hold the segments of the voltage sensor together (18), an observation that can be transposed to our models of NaChBac. D-58, which is located near the extracellular end of S2, stands alone near S3b and S4. It binds these two segments together near their respective hinges (N-terminal end of segment S3b and C-terminal end of segment S4) and may allow the S3b-S4 hairpin to move like a trap door. E-68 and D-91 are located close to each other and have similar biophysical characteristics and similar interactions in the models. These residues hold S2 and L4-5 (E-68-R-129) and S2 and S3 near the intracellular side of the membrane (R-72-D-91) together, respectively. They also may hold the intracellular part of the voltage sensor domain tightly together, whereas D-58 creates a ''door hinge'' that allows a controlled movement of S3b and S4. Most of the other published modeling and structural studies do not provide extensive discussions of the possible role of these residues.

Hypotheses about the role of S2-S3 acidic residues in the voltage-sensor domain

Are the acidic residues in S2 and S3 involved in the voltage-sensing process like the arginine residues in S4? A previous study suggested that E-293 in the *Shaker* K+ channel (E-68 in NaChBac) may be involved in voltage sensing (12). Although we observed changes in the slope factors, this does not definitively mean that E-68 is involved in voltage sensing. To unravel this effect, gating current measurements

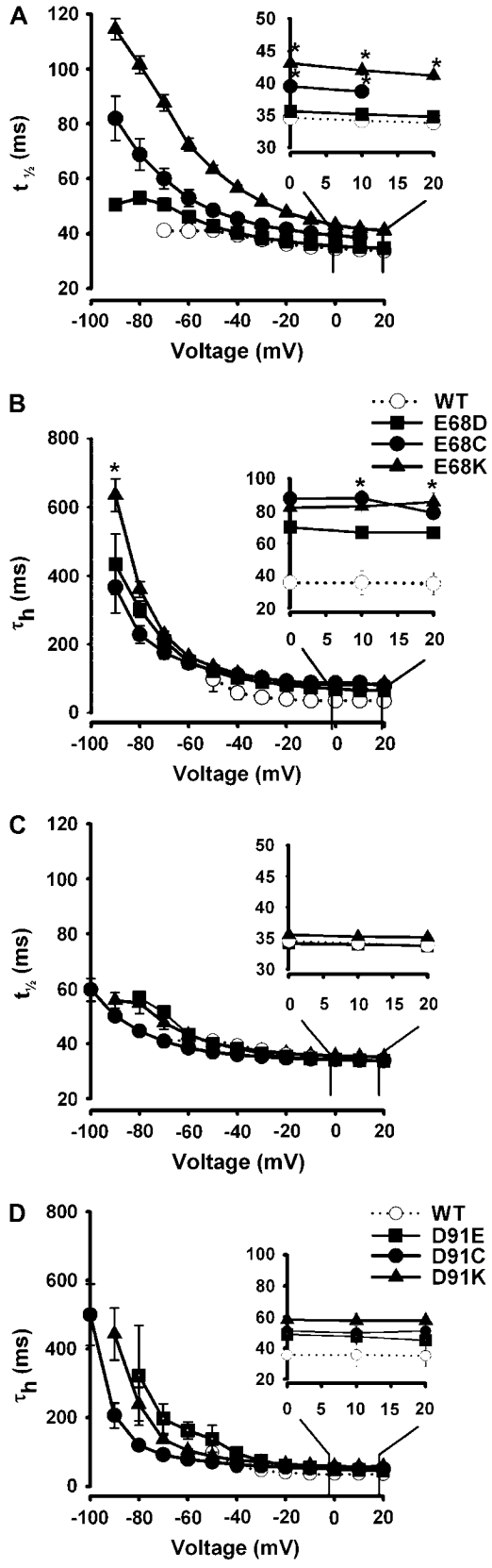

FIGURE 6 Voltage-dependence of the time constants of activation and inactivation of mutants E-68 (*A* and *B*) and E-91 (*C* and *D*). The $t_{½}$ of the rising Na^+ currents (activation) and the decay of the Na^+ currents (inactivation) fitted with single exponentials were determined. The values of the $t_{½}$ of activation and the τ_h of inactivation obtained were plotted versus the voltage. The values are expressed as mean ± SE for $n \geq 4$. Zoom of the three last time constants with significant differences ''*'' ($p < 0.05$) can be seen in the inset at the right top of each panel. The dashed line and open symbols correspond to the NaChBac/WT channel. The values of the $t_{½}$ of activation and the τ_h of inactivation for E-68C and E-68D showed significant differences from WT ($p < 0.05$) at different voltage values ranging from −60 mV to 10 mV.

are required. The NaChBac models showed that the mutations altered the interaction patterns inside the domain and might also have modified the way the voltage sensor moves during gating. It is clear from the models that mutations changed specific interactions with other segments of the voltage-sensor domain. For example, mutating E-68 to C or K in NaChBac slowed the kinetics of both activation and inactivation to a degree very similar to that previously observed for R-129C (10). This was predicted by our model. Indeed, in the model, E-68 and R-129 interacted strongly (Fig. 7 *F*). When the charge of one or the other residue was changed, this disturbed the interaction between the residues and slowed the kinetics of the channel.

If residue-residue interactions are the key factor in the movement of voltage sensors, it follows that mutations of negatively charged residues in S2-S3 segments will destabilize the structure and affect the ''dynamic equilibrium'' of the domain. These changes, even when they only slightly affect the local structure, can have a considerable effect on the way the sensor moves by making the structure either more flexible or more rigid and by altering the biophysical characteristics. When D-58 is mutated into E-58, its interactions with S4 are stronger and the hinge would be held more tightly. This would stabilize the S3b-S4 hairpin (the paddle), which would then react with a relatively smaller change in the membrane potential. Mutating D-58 to C or K weakens the interactions, and the paddle becomes more awry in its movement. Residue 58 cannot hold S3b-S4 together and a larger section of the paddle is allowed to move, requiring a larger potential difference to open the channel. This is consistent with the observed shift to the right of the G-V curve. Mutations at position 68 destroy (C or K) or reduce (D) its interaction with R-129 (L4-5). With the two first mutations, the L4-5 segment is no longer attached to S2 and can transfer the movement of the sensor (from S4) more easily to the pore through the S6 segment, while requiring a smaller potential difference, which would result in the observed leftward shift of activation. However, this structure is unstable and has difficulty returning to the resting conformation, which might explain the slower inactivation decay. Reducing the interaction force with E-68D might, in fact, allow a stronger interaction between R-129 and D-91, just as D-91E interacts more strongly with R-129. This change in interaction strength would affect the movement of

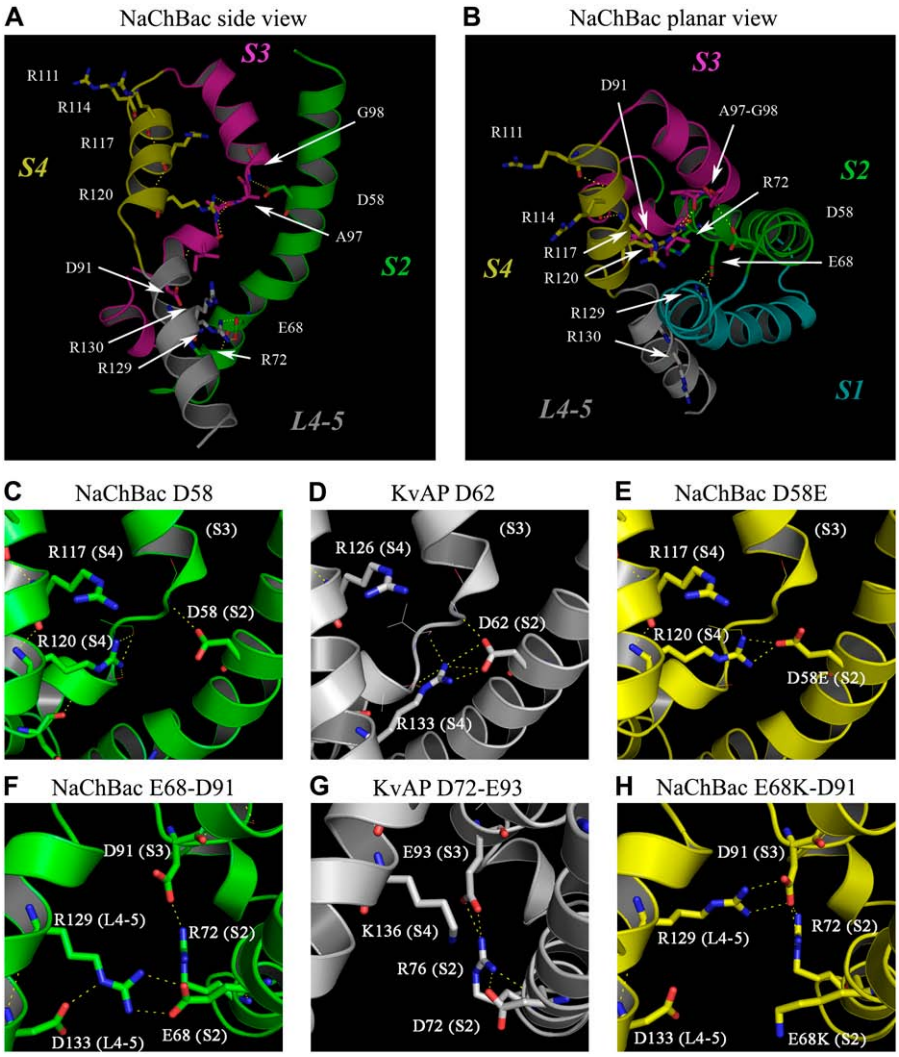

FIGURE 7 NaChBac's voltage-sensor domain and close-up view of main residue-residue interactions. (*A*) Side view of the voltage sensor used for close-ups of residue D-58 (*C–E*, below). S1 was removed from the picture for more clarity. Segments are identified by colors: S1 (absent) is cyan, S2 is green, S3 is magenta, S4 is yellow, and the S4-S5 linker segment is gray. Important residues of our study are represented as sticks, and yellow dashed lines represent strong electrostatic interactions. The gap observed in S3 is caused by inserted residues in NaChBac that were not introduced in the model, and the deletion of a residue in S4 causes a helix break, which might correspond to the junction between S4 and L4-5 (see Fig. 1 for insertions-deletions and Methods in Supplementary Material). (*B*) Planar view of the voltage sensor used for close-ups of residues E-68 and D-91 (*F–H*, see below). Segments use the same color code as described above. (*C*) D-58 mainly interacted with the backbone of G-98 in S3b. R-120 interacted with L-93, I-94, and A-96. (*D*) In KvAP, D-62 (homologous to D-58) interacted with the backbone of S3b and R-133 in S4. R-133 is homologous to R-120 in NaChBac and K-374 in *Shaker*. (*E*) Mutant D-58E maintained a good interaction with G-98 but also interacted more strongly with R-120, which had weaker interactions with I-94 and A-96. (*F*) E-68 mainly interacted with R-129 in S4, and D-91 with R-72. (*G*) In KvAP, D-72 (homologous to E-68) and E-93 (homologous to D-91) mainly interacted with R-76 (homologous to R-72), whereas K-136 (homologous to R-129) appeared too far away to interact with the acidic residues. (*H*) E-68K no longer interacted with R-129, which was pushed toward D-91 and formed a strong salt bridge.

the L4-5 segment, which would then require a relatively stronger change in potential (more gating energy) to alter the conformation of the pore. Mutating D-91 to C or K destroys its interaction with R-72, which would decrease the stability of S2, which in turn would then move with L4-5 due to a stronger interaction between E-68 and R-129.

TABLE 2 List of the strongest interactions of the WT residues with their environments (in kcal·mol^{-1})

	Total	VdW	Electro
D-58-E-41	4.0	0.0	4.0
D-58-A-97	−2.2	−0.3	−1.9
D-58-G-98	−3.6	−0.7	−2.8
D-58-R-120	−7.1	−0.1	−7.0
E-68-R-72	−14.7	−1.3	−13.0
E-68-D-91	4.7	−0.1	4.8
E-68-R-129	−36.7	1.6	−37.5
E-68-D-133	5.1	0.0	5.1
D-91-E-68	4.7	−0.1	4.8
D-91-R-72	−24.1	0.4	−24.2
D-91-R-120	−3.2	−0.1	−3.1
D-91-R-129	−5.9	−0.1	−5.8

These interactions were selected with an energy cutoff of ±3.0 kcal·mol^{-1} and do not include intramolecular interactions like α-helix H-bonds.

The voltage sensor of NaChBac seemed to influence the process of channel inactivation, unlike what has been suggested by Pavlov et al. (3). Chahine et al. (10) reported that mutating the arginine residues in S4, especially R-120 (R-4), dramatically slows the kinetics of inactivation of the channel, as was the case for E-68 (and D-91 to a lesser extent) in this study. This has not been observed with other channels and could, in fact, be another difference between NaChBac and other known channels (6–8,33). However, this may simply be due to the different mechanisms governing inactivation. Further studies are required to elucidate the molecular determinants of the inactivation process of NaChBac.

As well as playing a role in the stability and dynamics of the voltage sensor, the acidic residues in S2-S3 may have an influence on the local electric field. Electrostatic forces are long-range interactions and can have an influence on crystal structure that molecular modeling cannot characterize. In addition, we do not know exactly how the charges on S4

TABLE 3 Residue-residue interaction energy differences (Δ kcal·mol^{-1}) between the WT and the mutants (see Table 2 for WT energy values)

	WT	D-58C	D-58K	D-58E	E-68C	E-68K	E-68D	D-91C	D-91K	D-91E
D-58-E-41	0.0	−4.0	**−34.5**	1.1	−0.1	−0.6	−0.7	−0.5	−0.5	−0.7
D-58-A-97	0.0	2.2	2.2	−0.8	−0.8	0.1	0.2	−0.8	2.2	−0.6
D-58-G-98	0.0	3.6	3.6	−0.2	−1.7	0.1	0.4	−0.9	0.7	−1.1
D-58-R-120	0.0	**7.1**	**7.1**	**−25.2**	−2.5	−0.2	−2.5	−0.8	1.1	**−5.1**
E-68-R-72	0.0	**6.1**	2.6	**5.1**	**14.7**	**14.7**	−2.1	**−18.2**	**−18.6**	2.2
E-68-D-91	0.0	−0.8	−0.2	−1.0	−4.7	−4.7	0.2	−4.7	**−14.8**	1.1
E-68-R-129	0.0	−0.2	−0.1	**5.4**	**36.7**	**36.7**	**9.3**	−0.2	1.0	4.0
E-68-D-133	0.0	0.0	0.4	−0.2	**−5.1**	**−5.1**	−0.8	0.1	0.2	0.2
D-91-E-68	0.0	−0.8	−0.2	−1.0	−4.7	−4.7	0.2	−4.7	**−14.8**	1.1
D-91-R-72	0.0	**−5.6**	−2.1	−0.7	−0.5	**−7.1**	0.6	**24.1**	**31.8**	**−12.9**
D-91-R-120	0.0	0.1	0.1	3.2	0.1	0.0	0.1	3.2	3.2	3.2
D-91-R-129	0.0	0.9	0.3	1.3	1.5	**−28.9**	0.0	**5.9**	**14.9**	−2.8

Because some energy values from the mutants were outside the ±3.0 kcal·mol^{-1} cutoff, their interaction energy is considered to be zero; in this table, such a result gives a value equivalent to the WT with the opposed sign (like interaction D-58-A-97 in D-58C, etc.).

move through the electric field nor what form or length it has. It has already been shown that small changes in focused electric fields can affect gating (34).

Role of residue-residue interactions during gating

If residue-residue interactions are vital in maintaining a functioning sensor, it is important to know whether such interactions change from one conformation to another. Because we only built a model of the activated conformation (see Materials and Methods), the interactions of the resting conformation in NaChBac could not be observed. As mentioned above, relatively little is known about the structure-function of the resting conformation of most ion channels, and what information exists is generally incomplete or contradictory. If the gating movement is large (35), then the interactions will certainly change. Most probably, the salt bridges posited in the models will break and new ones will form (36). If the gating movement is small or if the salt bridges we described (D-58-R-120, E-68-R-129, and D-91-R-72) are stable, breaking the salt bridges would be energetically unfavorable in terms of allowing a reaction as fast as that observed with voltage sensing. The interactions should thus remain almost unchanged between the resting and the activated conformations. However, two theoretical studies have recently described models that reconcile the contradictory experiments in that they allow for a smaller, lateral displacement of the S4 segment together with a displacement large enough to change the interactions of the S2-S3 acidic residues (37,38).

CONCLUSION

We studied the effect of mutating conserved acidic residues in segments S2 and S3 of the NaChBac sodium channel. It is clear from the experimental data and the structural models that these residues are important for voltage-sensor functions. Although they are conserved in every known voltage sensor (7), very little is known about their role in voltage sensing (11–13,32). Molecular modeling suggests that specific interactions between residues of different segments are very important, whether for maintaining domain stability or local electric fields, or both. These interactions in NaChBac are D-58 (S2) with A-97-G-98 (S3) and R-120 (S4), E-68 (S2) with R-129 (L4-5), and D-91 (S3) with R-72 (S2), which is also a conserved residue. Our results provide support for the modeled interaction between E-68 and R-129, which shows that this link between the S2 segment and the S4-S5 linker of NaChBac is important for channel function and kinetics. These interactions seem to act like strap hinges that stabilize the voltage-sensor domain. A similar role for these interactions has also been suggested in KvAP (18). However, this hypothesis is not supported by a possible large movement of the voltage-sensor (35) where these interactions change between the closed and open conformations, unless the movement of S4 is characterized by a lateral displacement (37–39). Although the crystal structures of the voltage sensors of KvAP and Kv1.2 have shed some light on their interactions in the open conformation, we still do not know much about their configurations in the closed conformation. More information on the structure of the closed conformation would certainly help determine the role of these residues in addition to the length of the voltage-sensor movement.

SUPPLEMENTARY MATERIAL

An online supplement to this article can be found by visiting BJ Online at http://www.biophysj.org.

This study was supported by grants from the Heart and Stroke Foundation of Québec and the Canadian Institutes of Health Research. M. Chahine is an Edwards Senior Investigator (Joseph C. Edwards Foundation).

REFERENCES

1. Hille, B. 2001. Ion channels of excitable membranes. Sinauer Associates, Sunderland, MA.

2. Ren, D., B. Navarro, H. Xu, L. Yue, Q. Shi, and D. E. Clapham. 2001. A prokaryotic voltage-gated sodium channel. *Science*. 294:2372–2375.
3. Pavlov, E., C. Bladen, R. Winkfein, C. Diao, P. Dhaliwal, and R. J. French. 2005. The pore, not cytoplasmic domains, underlies inactivation in a prokaryotic sodium channel. *Biophys. J.* 89:232–242.
4. Yue, L., B. Navarro, D. Ren, A. Ramos, and D. E. Clapham. 2002. The cation selectivity filter of the bacterial sodium channel, NaChBac. *J. Gen. Physiol.* 120:845–853.
5. Long, S. B., E. B. Campbell, and R. MacKinnon. 2005. Voltage sensor of Kv1.2: structural basis of electromechanical coupling. *Science*. 309: 903–908.
6. Murata, Y., H. Iwasaki, M. Sasaki, K. Inaba, and Y. Okamura. 2005. Phosphoinositide phosphatase activity coupled to an intrinsic voltage sensor. *Nature*. 435:1239–1243.
7. Sasaki, M., M. Takagi, and Y. Okamura. 2006. A voltage sensor-domain protein is a voltage-gated proton channel. *Science*. 312:589–592.
8. Ramsey, I. S., M. M. Moran, J. A. Chong, and D. E. Clapham. 2006. A voltage-gated proton-selective channel lacking the pore domain. *Nature*. 440:1213–1216.
9. Bezanilla, F. 2000. The voltage sensor in voltage-dependent ion channels. *Physiol. Rev.* 80:555–592.
10. Chahine, M., S. Pilote, V. Pouliot, H. Takami, and C. Sato. 2004. Role of arginine residues on the S4 segment of the *Bacillus halodurans* Na^+ channel in voltage-sensing. *J. Membr. Biol.* 201:9–24.
11. Papazian, D. M., X. M. Shao, S. A. Seoh, A. F. Mock, Y. Huang, and D. H. Wainstock. 1995. Electrostatic interactions of S4 voltage sensor in *Shaker* K^+ channel. *Neuron.* 14:1293–1301.
12. Seoh, S. A., D. Sigg, D. M. Papazian, and F. Bezanilla. 1996. Voltage-sensing residues in the S2 and S4 segments of the *Shaker* K^+ channel. *Neuron.* 16:1159–1167.
13. Tiwari-Woodruff, S. K., C. T. Schulteis, A. F. Mock, and D. M. Papazian. 1997. Electrostatic interactions between transmembrane segments mediate folding of *Shaker* K+ channel subunits. *Biophys. J.* 72:1489–1500.
14. Keynes, R. D., and F. Elinder. 1999. The screw-helical voltage gating of ion channels. *Proc. R. Soc. Lond. B Biol. Sci.* 266:843–852.
15. Pradhan, P., R. Ghose, and M. E. Green. 2005. Voltage gating and anions, especially phosphate: a model system. *Biochim. Biophys. Acta*. 1717:97–103.
16. Green, M. E. 2005. A possible role for phosphate in complexing the arginines of S4 in voltage gated channels. *J. Theor. Biol.* 233:337–341.
17. Jiang, Y., A. Lee, J. Chen, V. Ruta, M. Cadene, B. T. Chait, and R. MacKinnon. 2003. X-ray structure of a voltage-dependent K^+ channel. *Nature*. 423:33–41.
18. Monticelli, L., K. M. Robertson, J. L. MacCallum, and D. P. Tieleman. 2004. Computer simulation of the KvAP voltage-gated potassium channel: steered molecular dynamics of the voltage sensor. *FEBS Lett.* 564:325–332.
19. Kumar, S., and R. Nussinov. 2002. Close-range electrostatic interactions in proteins. *ChemBioChem.* 3:604–617.
20. Margolskee, R. F., B. McHendry-Rinde, and R. Horn. 1993. Panning transfected cells for electrophysiological studies. *Biotechniques.* 15: 906–911.
21. Jurman, M. E., L. M. Boland, Y. Liu, and G. Yellen. 1994. Visual identification of individual transfected cells for electrophysiology using antibody-coated beads. *Biotechniques.* 17:876–881.
22. Chenna, R., H. Sugawara, T. Koike, R. Lopez, T. J. Gibson, D. G. Higgins, and J. D. Thompson. 2003. Multiple sequence alignment with the Clustal series of programs. *Nucleic Acids Res.* 31:3497–3500.
23. Notredame, C., D. G. Higgins, and J. Heringa. 2000. T-Coffee: a novel method for fast and accurate multiple sequence alignment. *J. Mol. Biol.* 302:205–217.
24. Zhorov, B. S., and P. D. Bregestovski. 2000. Chloride channels of glycine and GABA receptors with blockers: Monte Carlo minimization and structure-activity relationships. *Biophys. J.* 78:1786–1803.
25. Zhorov, B. S. 1983. Topography of the active site of the noradrenaline neuronal membrane carrier based on the theoretical conformation analysis of inhibitors of neuronal catecholamine uptake. *Bioorg. Khim.* 9:200–215.
26. Weiner, S. J., P. A. Kollman, D. A. Case, U. C. Singh, C. Ghio, G. Alagona, S. Profeta Jr., and P. Weiner. 1984. A new force field for molecular mechanical simulation of nucleic acids and proteins. *J. Am. Chem. Soc.* 106:765–784.
27. Brooks, C. L. I., B. M. Pettitt, and M. Karplus. 1985. Structural and energetic effects of truncating long ranged interactions in ionic and polar fluids. *J. Chem. Phys.* 83:5897–5908.
28. Lazaridis, T., and M. Karplus. 1999. Effective energy function for proteins in solution. *Proteins.* 35:133–152.
29. Li, Z., and H. A. Scheraga. 1987. Monte Carlo-minimization approach to the multiple-minima problem in protein folding. *Proc. Natl. Acad. Sci. USA.* 84:6611–6615.
30. Zhorov, B. S., and V. S. Ananthanarayanan. 1996. Structural model of a synthetic Ca^{2+} channel with bound Ca^{2+} ions and dihydropyridine ligand. *Biophys. J.* 70:22–37.
31. Zhorov, B. S., and S. X. Lin. 2000. Monte Carlo-minimized energy profile of estradiol in the ligand-binding tunnel of 17 beta-hydroxysteroid dehydrogenase: atomic mechanisms of steroid recognition. *Proteins.* 38:414–427.
32. Planells-Cases, R., A. V. Ferrer-Montiel, C. D. Patten, and M. Montal. 1995. Mutation of conserved negatively charged residues in the S2 and S3 transmembrane segments of a mammalian K^+ channel selectively modulates channel gating. *Proc. Natl. Acad. Sci. USA.* 92: 9422–9426.
33. Long, S. B., E. B. Campbell, and R. MacKinnon. 2005. Crystal structure of a mammalian voltage-dependent *Shaker* family K^+ channel. *Science*. 309:897–903.
34. Starace, D. M., and F. Bezanilla. 2004. A proton pore in a potassium channel voltage sensor reveals a focused electric field. *Nature*. 427: 548–553.
35. Ruta, V., J. Chen, and R. MacKinnon. 2005. Calibrated measurement of gating-charge arginine displacement in the KvAP voltage-dependent K^+ channel. *Cell.* 123:463–475.
36. Kumar, S., and R. Nussinov. 1999. Salt bridge stability in monomeric proteins. *J. Mol. Biol.* 293:1241–1255.
37. Treptow, W., and M. Tarek. 2006. Environment of the gating charges in the Kv1.2 *Shaker* potassium channel. *Biophys. J.* 90:L64–L66.
38. Yarov-Yarovoy, V., D. Baker, and W. A. Catterall. 2006. Voltage sensor conformations in the open and closed states in ROSETTA structural models of K(+) channels. *Proc. Natl. Acad. Sci. USA.* 103:7292–7297.
39. Elliott, D. J. S., E. J. Neale, Q. Aziz, J. P. Dunham, T. S. Munsey, M. Hunter, and A. Sivaprasadarao. 2004. Molecular mechanism of voltage sensor movements in a potassium channel. *EMBO J.* 23: 4717–4726.
40. Blunck, R., D. M. Starace, A. M. Correa, and F. Bezanilla. 2004. Detecting rearrangements of *Shaker* and NaChBac in real-time with fluorescence spectroscopy in patch-clamped mammalian cells. *Biophys. J.* 86:3966–3980.